

Electronic Supplementary Information

Sub-nL Thin-film Differential Scanning Calorimetry Chip for Rapid Thermal Analysis of Liquid Samples

Sheng Ni,^a Hanliang Zhu,^c Pavel Neuzil,^c and Levent Yobas^{a,b,*}

^a Department of Electronic and Computer Engineering, The Hong Kong University of Science and Technology, Clear Water Bay, Kowloon, Hong Kong SAR, China

^b Department of Chemical and Biological Engineering, The Hong Kong University of Science and Technology, Clear Water Bay, Kowloon, Hong Kong SAR, China

^c The Ministry of Education Key Laboratory of Micro/Nano Systems for Aerospace, Department of Microsystem Engineering, School of Mechanical Engineering, Northwestern Polytechnical University, Xi'an, 710072, China

* To whom correspondence should be addressed. Phone: +852-2358 7068. Fax: +852-2358 1485. E-mail: eelyobas@ust.hk

Contents:

Experimental Setup	S-3
Readout Unit	S-4
Extraction of Thermal Parameters	S-5
Thermograms from single heating-cooling cycles	S-8
Symmetry Verification	S-9
Benchmarking	S-9
References	S-13

Experimental Setup

Fig. S-1a shows a photograph of sub-nL tfDSC chip mounted on a PCB and an optical micrograph of the overall chip. Fig. S-1b depicts an exploded view of the custom-made vacuum chamber used in experiments. The vacuum chamber also served as a Faraday cage for readout electronics and contained a thermal enclosure for further isolation of the prepared sub-nL tfDSC chip. The parts that are not shown are the turbomolecular pump (Turbo-V70, Varian, Lexington, MA) used for establishing the vacuum and the Styrofoam box housing the vacuum chamber with ice packs (NOR1038, Nordic Cold Chain Solutions, Reno, NV) for bringing the onset temperature down to about 10 °C.

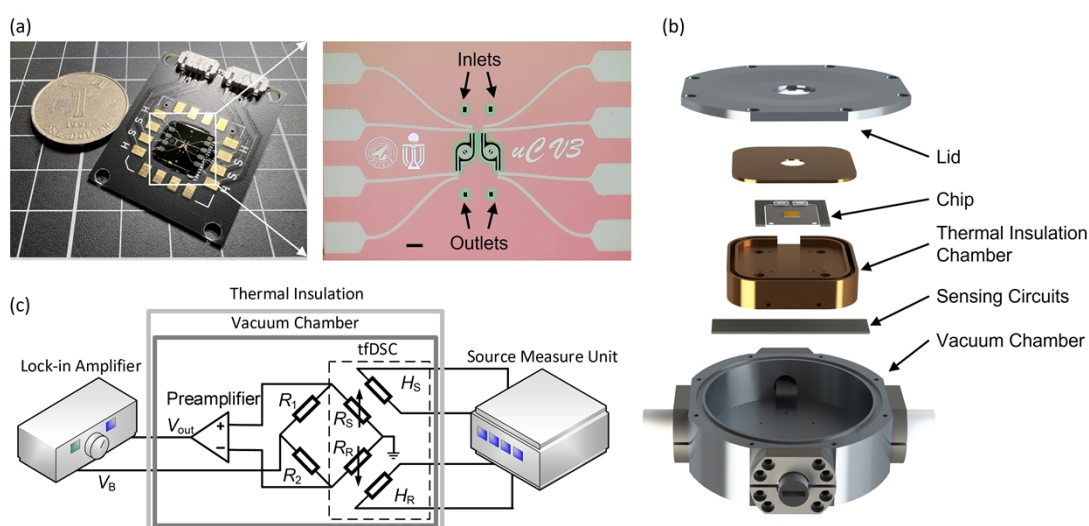


Fig. S-1. Sub-nL tfDSC chip and experimental setup. (a) Photograph of the chip mounted on a PCB shown next to a coin and an optical micrograph of the overall chip in plane view (scale: 500 μm). (b) Exploded view of the custom-made vacuum chamber and (c) simplified diagram of the readout circuit used in the measurements. It featured a dual-channel source measure unit, a differential preamplifier, a lock-in amplifier and a Wheatstone bridge with R_1 and R_2 as the balancing resistors. The resistors, H_S and H_R , denote the thin-film heaters on the sample and reference arms and the resistors, R_S and R_R , the corresponding RTDs, respectively.

Readout Unit

Fig. S-1c shows a simplified diagram of the unit including the circuit and instrumentation. As described, the unit is based on the lock-in amplification with a source measure unit supplying the required power to the resistive heaters, H_S and H_R integrated on the sample and references arms. The unit also features a Wheatstone bridge and a differential amplifier for measuring the differential temperature of the arms through their RTDs represented by the variable resistors, R_S and R_R .

Fig. S-2a depicts the readout circuit on a PCB. The corresponding circuit diagram is presented in Fig. S-2b. In the Wheatstone bridge, we included an additional branch which we referenced against the other two branches during balancing the bridge. By referencing the node P_3 , we first tuned the variable resistor R_2 to null the amplified peak voltage ΔV^* . Similarly, by referencing the node P_2 , we tuned the variable resistor R_1 to null the amplified peak voltage ΔV , the output where we obtained thermograms. We used differential amplifiers type AD8221BRZ (Analog Devices, Norwood, MA).

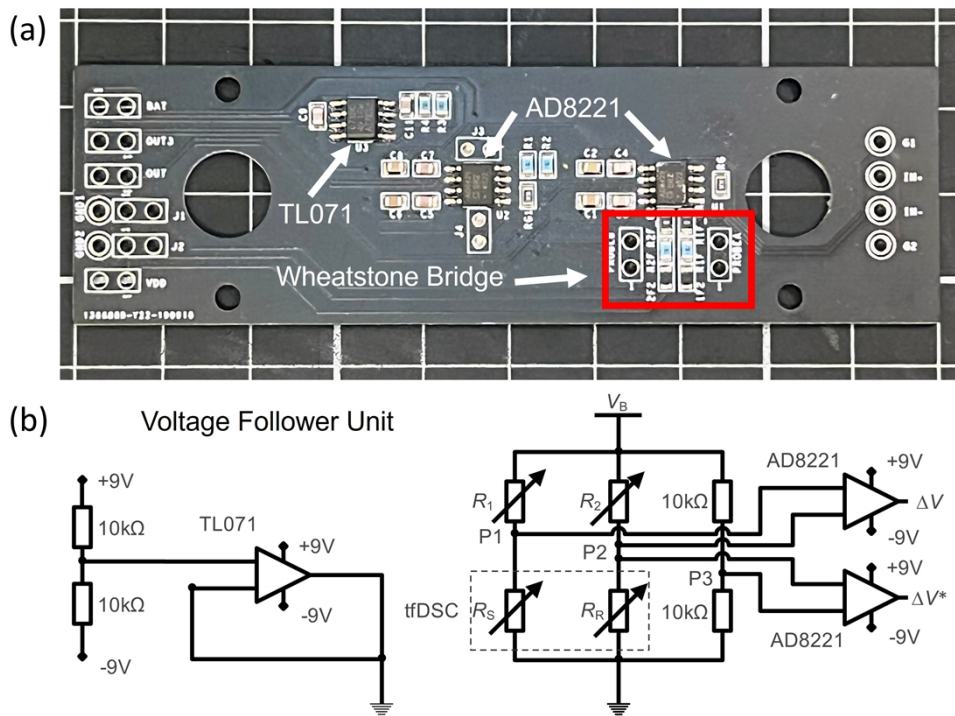


Fig. S-2. (a) Photograph of the readout circuit on a PCB and (b) its circuit diagram. The circuit consists of a Wheatstone bridge and a pair of differential preamplifiers with all nodes referenced to a virtual ground provided by a voltage follower unit.

To power amplification circuits, we used two 9 V batteries (MN1604, Duracell, CT) connected in series. We referenced all circuit nodes to a virtual ground generated by a voltage follower unit (TL071, Texas Instruments, Dallas, TX), which is also described in Fig. S-2b. We biased the Wheatstone bridge using a sinewave voltage at about 1 kHz and 100 mV peak from a lock-in amplifier (HF2IS, Zurich Instrument, Zurich, Switzerland). We balanced the bridge under vacuum at an ambient temperature of about 10 °C immediately before a temperature scan. We kept the variable resistors R_1 and R_2 outside the vacuum chamber and connected to the bridge via vacuum feedthroughs.

Extraction of Thermal Parameters

We extracted the thermal parameter values of twin arms using the long pulse method as described in our previous work.¹ Briefly, we extracted the values of the heat conduction, G_r and thermal time constant τ of the arms using a quarter Wheatstone bridge featuring the RTD of the arm under test and a variable balancing resistor R_1 , along with a pair of fixed resistors R , each at a value of 10 k Ω (Fig. S-3a). We applied a series of voltage pulses to the bridge from a function generator (DG1022, Rigol Technologies, Beijing, China) while recording the pulse waveform and the amplified bridge output V_{out} on an oscilloscope (TBS 1072B-EDU, Tektronix, Beaverton, OR). We set a gain of 991 through the differential amplifier (AD8221BRZ).

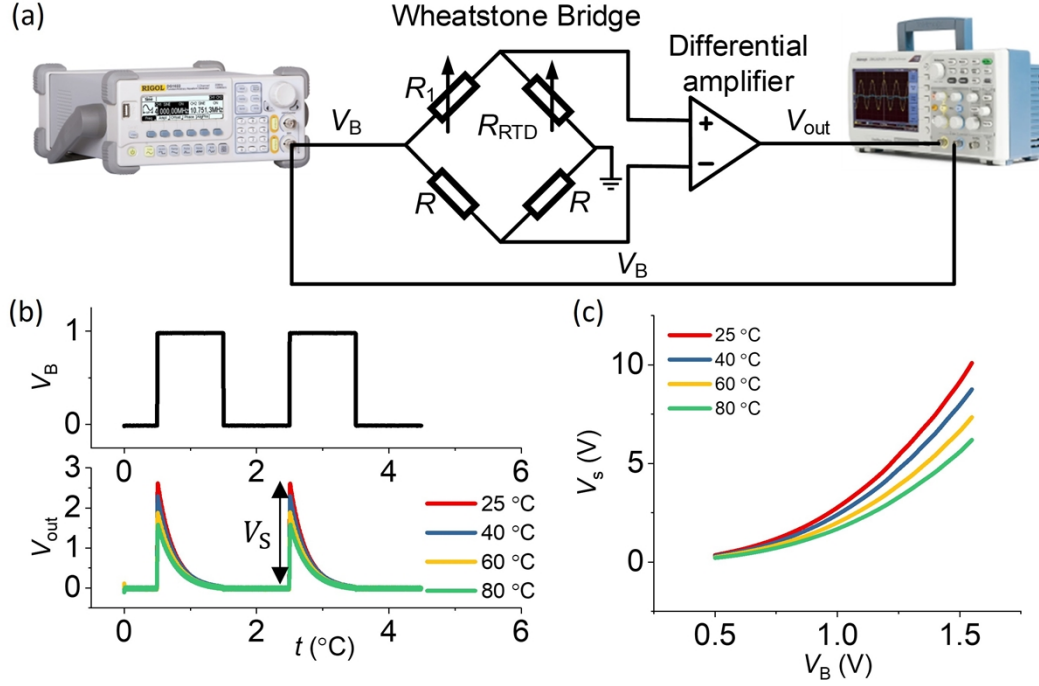


Fig. S-3. Extraction of thermal parameter values. (a) The Wheatstone bridge diagram. (b) Representative recordings of V_{out} for the applied voltage pulse pair of an amplitude V_B and for the set temperatures of the arm (legend). (c) Plot of the steady-state voltage V_s as denoted in (b) against V_B for the set temperatures of the arm (legend).

We repeated each measurement for a fixed value of the arm temperature with the integrated heater supplied from a source measure unit (Keithley 2612B, Tektronix, Beaverton, OR). Fig. S-4b shows a set of representative measurements for select values of the arm temperature (legend) and for the pulse pair applied at an amplitude of $V_B = 1$ V. We set the pulse period and duty cycle as 2 s and 50% to allow for sufficient heating and cooling time depending on the τ value of the arm. For a select value of the arm temperature, we determined the τ value as well as the magnitude of V_s (defined in the V_{out} trace) through a curve fitting according to:

$$V_{out} = 991 \times \left\{ V_0 + V_s \left[1 - \exp\left(-\frac{t - t_0}{\tau} \right) \right] \right\} \quad (\text{S-1})$$

where V_0 and t_0 represent the offset voltage and offset time, respectively. Subsequently, we repeated this procedure for the pulse amplitude V_B set to 0.5 and 1.55 V and then obtained the

plot of V_S as a function V_B (Fig. S-4c). From this plot, we determined the G_r value as a function of the arm temperature through a polynomial curve fitting:

$$V_S = V_0' + \frac{\alpha}{16G_r R} V_B^3 \quad (\text{S-2})$$

where V_0' is the offset voltage, α the TCR, and R the RTD resistance measured at the corresponding arm temperature.

Thermograms from single heating-cooling cycles

tfDSC thermograms of 5CB and 7CB obtained during single heating-cooling cycles between 10 °C and 100 °C performed at identical scan rates are separately presented for the heating and cooling segments in Fig. S-4.

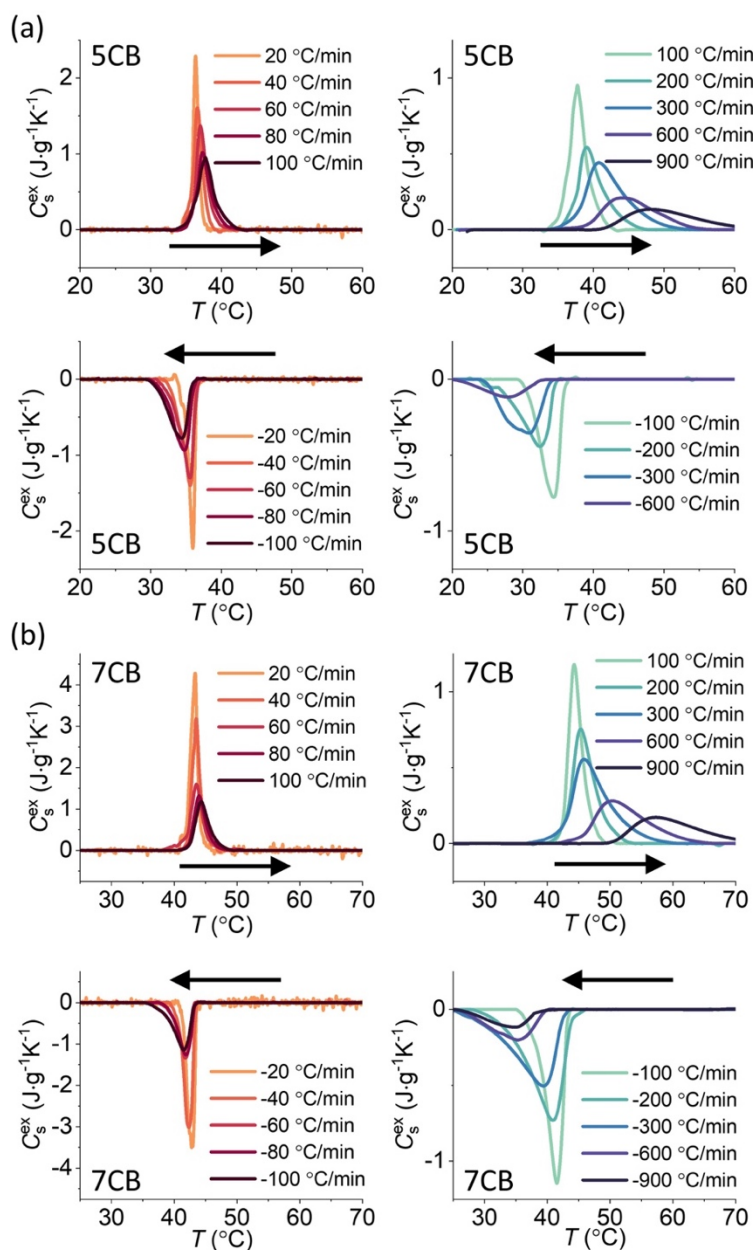


Fig. S-4. The influence of tfDSC scan rate on the excess heat capacity peaks obtained during the phase transitions of (a) 5CB and (b) 7CB: the N-I phase transitions (endothermic peaks) during heating (upper panels) and the I-N phase transitions (exothermic peaks) during subsequent cooling (lower panels).

Symmetry Evaluation

The plots of the phase transition peak temperature T_p values of 5CB and 7CB as a function of the temperature scan rate obtained from Fig.S-4 are presented in Fig. S-5 for the evaluation of thermal lag symmetry. For thermal lag symmetry, the fitting lines for heating and cooling data should ideally have the same slope values. The slope values are very close in the case of 5CB: 0.01416 min (0.85 s) for heating and 0.01476 min (0.89 s) for cooling. In the case of 7CB, the slope values slightly differ but the deviation from symmetry is small: 0.0117 min (0.70 s) for heating and 0.01372 min (0.82 s) for heating and 0.01372 min (0.82 s).

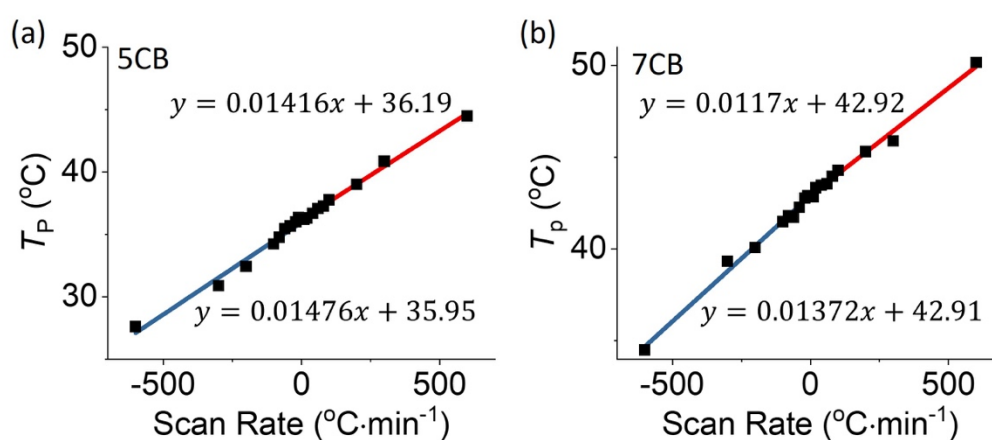


Fig. S-5. The evaluation of thermal lag symmetry in heating and cooling: the plots of the scan rate versus the peak temperature T_p for (a) 5CB and (b) 7CB derived from the respective phase transition peaks in Fig. S-4. The lines and corresponding equations represent the best linear fits to heating data (red lines, $R^2 > 0.988$) and cooling data (blue lines, $R^2 > 0.975$).

Benchmarking

In Table S-1, we compare our tFDSC chip and the state-of-the-art DSC chips based on the technology used (sensor type and heating method), performance metrics reported (thermal time constant, temperature scan rate, sensitivity, and noise) and sample analyzed (type, volume, and concentration). Including this work, three studies have reported the use of on-chip heating for temperature scans and their resultant thermal time constant values are 1 s or less. Accordingly, this work along with the study on flash DSC² stand out in terms of scan rates >100 °C min⁻¹

while three other studies reported scan rates that exceed single digit degree per minute. Flash DSC and our chip also break away from the trend of others relating their temperature time constant and sensitivity (Fig. S-6). The sensitivity increases with the reduced heat conduction of the calorimeter, which is also responsible for the increased thermal response time unless the calorimeter thermal mass is proportionally reduced. As such, this trend is expected for temperature scans performed through off-chip heating, which typically introduce a large thermal mass. The sensitivity level reached here 11 V W^{-1} considerably exceeds the values reported by others while the noise level below 10 nW also compares favorably with those reports.

Table S-1. Benchmarking of the state-of-the-art DSC chips and conventional DSC for the calorimetry of liquid samples.

Ref	Author, Year	Sensor Type	On-chip Heating	Volume (nL)	Thermal Time Constant (s)	Scan Rate (°C/min)	Sensitivity (V/W)	Noise (nW)	Sample	Conc (mg/mL)
[3]	TA Nano DSC*	Thermopiles	N/A	300000	5	2	not mentioned	15	Lysozyme	0.007
[4]	Wang, 2008	Thermopile, Ni/Cr	No	1200	0.6	5	1.2	30	Lysozyme, Rnase A	20
[5]	Wang, 2011	Thermopile, Sb/Bi	No	1000	2.8	5	4	14	Lysozyme	1-20
[6]	Wang, 2013	Thermopile, Sb/Bi	No ‡	1000	2	5	8	-	Lysozyme	10-20
[7]	Jia, 2015	Thermopile, Sb/Bi	No	1000	2.6	5	4.78	21	Lysozyme	1-20
[8]	Wang, 2005	Thermopile, PolySi/Al	Yes	1000	1	5.4	2	-	Lysozyme	300
[9]	Wang, 2012	Thermopile, Sb/Bi	No	1000	2	6	4	10	Lysozyme	1-20
[10]	Wang, 2016	Thermistor, VOx	No	1000	6	7.5	6	40	Lysozyme	100
[11]	Wang, 2018	Thermistor, VOx	No†	1000	7.2	25	6	35	Lysozyme, BSA, mAb1	10
[12]	Yu, 2018	Thermistor, VOx	No	630	5.2	45	6.1	-	BSA	10
[13]	Yu, 2022	Thermistor, VOx	No	630	3.3	45	6.1	400	Lysozyme, mAb, Fab, DVD-Ig	10
[2]	Splinter, 2015	Thermopile, PolySi	Yes	10	0.1	400	5.5	<1000	Lysozyme	1-100
this work	Ni, 2022	RTD, Ti	Yes	0.4	0.6	900	11	7.7	Lysozyme, 5CB, 7CB	30-200

* Commercial DSC by TA Instruments.

‡ The research utilized on-chip heater for temperature modulation.

† The research utilized on-chip heater for power compensation.

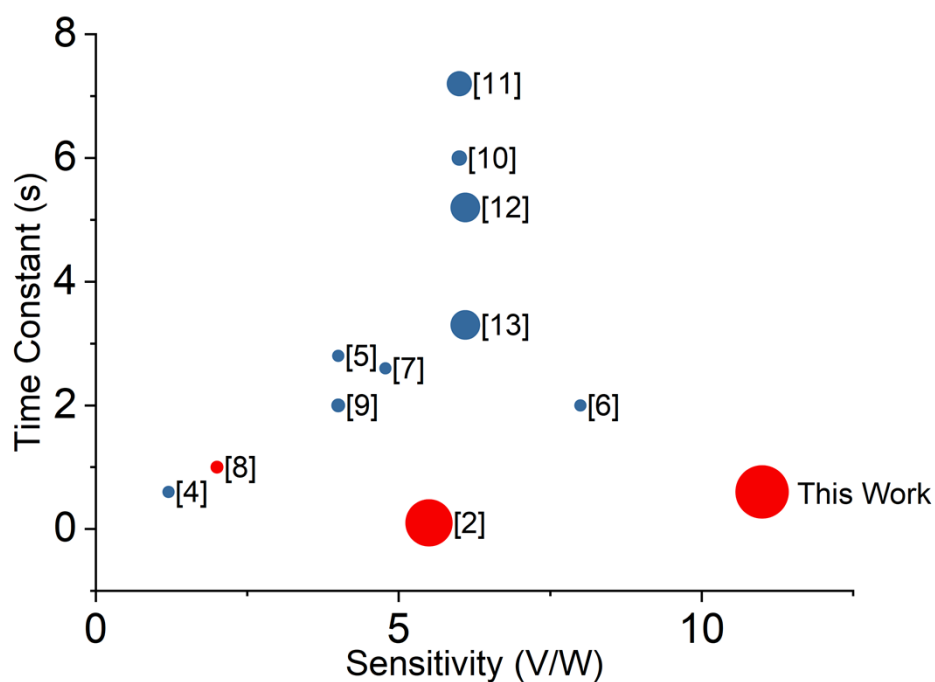


Fig. S-6. Map of the thermal time constant and sensitivity values of the state-of-the-art DSC chips for the calorimetry of liquid samples (from Table S-1). The size of each symbol signifies the applied scan rate in logarithmic scale ranging from $5\text{ }^{\circ}\text{C min}^{-1}$ to $900\text{ }^{\circ}\text{C min}^{-1}$. The symbol color represents the method of heating employed to establish linear scan rates with the blue color representing off-chip heating through either a thermal enclosure or a thermal stage and the red color representing on-chip heating through thin-film integrated heaters.

References

1. S. Ni, Y. Bu, H. Zhu, P. Neuzil and L. Yobas, *J. Microelectromech. Syst.*, 2021, **30**, 759-769.
2. R. Splinter, A. W. van Herwaarden, I. A. van Wetten, A. Pfreundt and W. E. Svendsen, *Thermochim. Acta*, 2015, **603**, 162-171.
3. Nano DSC, <https://www.tainstruments.com/nanodsc/>, (accessed Feb. 6th, 2023).
4. L. Wang, B. Wang and Q. Lin, *Sens. Actuators B Chem.*, 2008, **134**, 953-958.
5. B. Wang and Q. Lin, Proceedings of IEEE International Conference on Micro Electro Mechanical Systems (MEMS' 11), Cancun, Mexico, 2011.
6. B. Wang and Q. Lin, *Sens. Actuators B Chem.*, 2013, **180**, 60-65.
7. Y. Jia, B. Wang, Z. Zhang and Q. Lin, *Sens. Actuator A Phys.*, 2015, **231**, 1-7.
8. L. Wang, Y. J. Zhao, E. Ng and Q. Lin, Proceedings of IEEE International Conference on Micro Electro Mechanical Systems (MEMS' 05), Miami Beach, FL, USA, 2005.
9. B. Wang and Q. Lin, *J. Microelectromech. Syst.*, 2012, **21**, 1165-1171.
10. S. Wang, S. Yu, M. S. Siedler, P. M. Ihnat, D. I. Filoti, M. Lu and L. Zuo, *Rev. Sci. Instrum.*, 2016, **87**, 105005.
11. S. Wang, S. Yu, M. Siedler, P. M. Ihnat, D. I. Filoti, M. Lu and L. Zuo, *Sens. Actuators B Chem.*, 2018, **256**, 946-952.
12. S. Yu, S. Wang, M. Lu and L. Zuo, Proceedings of the ASME International Design Engineering Technical Conferences and Computers and Information in Engineering Conference, Quebec City, Canada, 2018.
13. S. Yu, Y. Wu, S. Wang, M. Siedler, P. M. Ihnat, D. I. Filoti, M. Lu and L. Zuo, *Biosensors (Basel)*, 2022, **12**, 422.